

Graphene-like Dirac states and Quantum Spin Hall Insulators in the square-octagonal MX_2 ($M=\text{Mo}, \text{W}$; $X=\text{S}, \text{Se}, \text{Te}$) Isomers

Yan Sun¹, Claudia Felser¹, and Binghai Yan^{1,2*}

¹ Max Planck Institute for Chemical Physics of Solids, 01187 Dresden, Germany and

² Max Planck Institute for the Physics of Complex Systems, 01187 Dresden, Germany
(Dated: September 5, 2018)

We studied the square-octagonal lattice of the transition metal dichalcogenide MX_2 (with $M=\text{Mo}, \text{W}$; $X=\text{S}, \text{Se}$ and Te), as an isomer of the normal hexagonal compound of MX_2 . By band structure calculations, we observe the graphene-like Dirac band structure in a rectangular lattice of MX_2 with nonsymmorphic space group symmetry. Two bands with van Hove singularity points cross each at the Fermi energy, leading to two Dirac cones that locates at opposite momenta. Spin-orbit coupling can open a nontrivial gap at these Dirac points and induce the quantum spin Hall (QSH) phase, the 2D topological insulator. Here, square-octagonal MX_2 structures realize the interesting graphene physics, such as Dirac bands and QSH effect, in the transition metal dichalcogenides.

PACS numbers: 73.20.At, 71.20.-b, 71.70.Ej

Since the discovery of graphene[1, 2], research about two dimensional (2D) materials has been widely explored in both theory and experiment. During the the last few years, transition metal dichalcogenides (TMD) MX_2 (with $M=\text{Mo}, \text{W}$ and $X=\text{S}, \text{Se}, \text{Te}$) [3, 4] have attracted extensive attention. For example, monolayer of MoS_2 is a direct-gap semiconductor and regarded as massive Dirac systems in the honeycomb lattice with interesting valley physics [5]. Very recently an isomer structure of MX_2 in the square-octagonal (so) lattice [11] was found to exhibit gapless band structure with a Dirac cone a the zone center, and lattice distortion [12] was claimed to remove above Dirac cone and induce additional band crossing at the Fermi energy. However, the topological feature in the band structure was neglected due to the missing of spin-orbital coupling in calculations. In this work, we revisited the square-octahedral lattices of MX_2 isomers, and discovered their graphene-like Dirac band structures (see Fig. 1) and the 2D topological insulator phase [6, 7].

Inspired by the atomic structures of grain boundaries in normal hexagonal MoS_2 [8–10], a square-octagon (so) lattice o for MoS_2 [11] was investigated in theory. There are four Mo atoms and eight S atoms in each primitive cell, as shown in Fig.1. And this lattice can be viewed as repeated square-octagon pairs in both x and y directions. Here, the trigonal prismatic structure of MoS_6 is slightly distorted compared to the hexagonal phase. Further, distortions from the square lattice to a rectangle lattice (distorted-so lattice) were found to optimize the strain in the 2D structure and realize more stable structures [12]. In this work, we adopted the similar lattice structures to TMD MX_2 (with $M=\text{Mo}$ and W ; $X=\text{S}, \text{Se}$ and Te) monolayers and found that the distorted-so-lattice is indeed the energetically favored structure for all compounds. The lattice distortion and total energy differences are summarized in Table I. We can see that for lattice distortion, characterized by the ratio of in-plane

lattice parameters b/a , becomes stronger as the increasing of atomic radius of atom X for fixed metal atom M , due to the elongated $M-X$ bond.

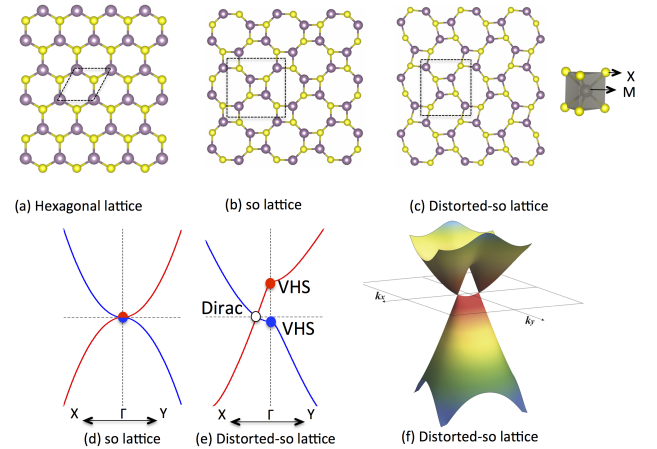


FIG. 1. (color online) Crystal lattice structure for MX_2 ($M = \text{Mo}, \text{W}$; $X = \text{S}, \text{Se}, \text{Te}$) in the (a) normal hexagonal lattice, (b) square-octagonal (so) lattice and (c) distorted-so lattice. The primitive unit cell is denoted by dashed lines. The band structures near the Fermi energy are illustrated in the 2D Brillouin zone for (d) so lattice, (e) distorted-so lattice. The 3D plot of the distorted-so lattice is shown in (f), where two Dirac cones forms in the $\Gamma - X$ line. The Dirac point and the van Hove singularity (VHS) point are indicated by empty and filled circles in (e), respectively.

We mainly focus on their topological electronic properties, after clarifying the lattice structures of MX_2 . Our calculations have been performed by using density functional theory (DFT) with projected augmented wave (PAW) method as implemented in the code of Vienna *Ab initio* Simulation Package (VASP) [13, 14]. The exchange-correlation energy are considered in the gener-

TABLE I. The lattice constants and electronic properties of MX_2 (with $M=Mo, W$; $X=S, Se$ and Te). Total energy differences between two types of lattices is defined as $\Delta E = E_{so-lattice} - E_{distorted-so-lattice}$ in one primitive cell. In the distorted-so-lattice, the linear band crossing at Fermi energy induces a Dirac cone, which locates on the line of Γ - X in the lattice momentum space. Its detailed location (k_D) is defined as the the relative distance away from Γ point, as the schematic diagram given in Fig.1(b). The ab -*initio* calculations for lattice structure optimization, total energy differences ΔE , and location of Dirac cone are performed without the inclusion of SOC, while for band gap E_g and Z_2 invariants the SOC was included.

	lattice constant (Å)		ΔE (meV)	E_g (meV)		Z_2 invariant		k_D ($\frac{2\pi}{a}$)
	so-lattice	distorted-so-lattice		so-lattice	distorted-so-lattice	so-lattice	distorted-so-lattice	
MoS ₂	$a=6.34$	$a=6.30, b=6.37$	0.68	25	12	1	1	0.025
MoSe ₂	$a=6.62$	$a=6.56, b=6.67$	1.11	38	23	1	1	0.073
MoTe ₂	$a=7.06$	$a=6.72, b=7.32$	17.87	49	19	1	1	0.201
WS ₂	$a=6.36$	$a=6.32, b=6.42$	1.26	111	64	1	1	0.072
WSe ₂	$a=6.64$	$a=6.30, b=6.88$	29.50	152	20	1	1	0.225
WTe ₂	$a=7.11$	$a=6.66, b=7.37$	87.20	213	19	1	1	0.245

alized gradient approximation (GGA) level with Perdew-Burke-Ernzerhof (PBE) based density functional [15]. The energy cutoff was set to be 350 eV. The tight binding matrix elements were calculated by projection Bloch states onto maximally localized Wannier functions (MLWFs) [17–19], using the VASP2WANNIER90 interface [20].

Because all the compounds of MX_2 share similar electronic properties, in the following part we will take MoS₂ and WS₂ as the examples for detailed analysis of their electronic structures. Band structures for two types of lattices are compared in Fig. 2. Without the inclusion of SOC effect, band structure in the so-lattice presents doubly degenerated d_{z^2} states at Γ point around the Fermi energy for both MoS₂ and WS₂, exhibiting as a semi-metallic state. As long as the SOC is taken into consideration, the degenerated d_{z^2} bands split into two single states, with one locating at the top of valence band and the other up shifting to the second conduction band. Beside that, band anti-crossing between conduction and valence bands appears around Γ point, which implies the existence of band inversion.

In order to make clear the topological electronic properties, we analyzed the wave functions around the Fermi energy. As presented in Fig.2(a) and (d), the top of valence band and bottom of conduction bands at Γ point are mainly dominated by $M - d_{z^2}$ and $M - d_{x^2-y^2}$ orbitals, respectively, and these two states have opposite parities. Since the splitted two $M - d_{z^2}$ states are both with plus parities, the effect of SOC here is just opening the band gap but not changing topological band order. Because of the inversion symmetry in the so-lattice, we can directly achieve the topological number of Z_2 invariant by the products of parities at time reversal invariant momentas (TRIMs) [16]. The parity products for occupied states at the three independent TRIMs of $\Gamma(0,0)$, $X((0.5, 0), (0, 0.5))$ and $S(0.5, 0.5)$ are -, + and +, respectively, which gives the Z_2 invariant $\nu_0 = 1$. Therefore, it directly confirms the existence of QSH insulator state in the so- MX_2 .

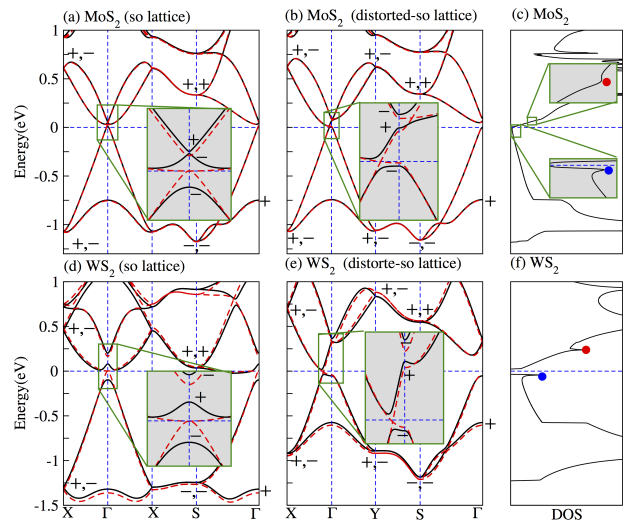


FIG. 2. (color online) Electronic band structures and density of states (DOS) for MoS₂ and WS₂. Energy dispersion along high symmetry lines in 2D BZ for (a, b) MoS₂ with so and distorted-so lattices, and (d, e) WS₂ with so and distorted-so lattices. (c) and (f) are total DOS for distorted-so MoS₂ and WS₂, respectively. Energy bands with (black solid lines) and without (red dot lines) are both included. DOS are calculated with the inclusion of SOC. Local band structures around Fermi energy are also given in the inserted figures. VHS points in the DOS are remarked with red and blue dots. Plus and minus signs remarked in band structures are the parity eigenvalues. Band structures are calculated from *ab-initio* method, and DOS are calculated from MLWFs. Fermi energy is set to be zero.

After the lattice distortion, the symmetry decreased from D_{2h} to C_{2h} , and one can expect a dramatically change of the electronic properties. As shown in Fig.2(b) and (e), doubly degenerated $M - d_{z^2}$ states at Γ point split for both MoS₂ and WS₂, even without the inclusion of SOC. Meanwhile, a linear band crossing forms a massless Dirac cone at the Fermi level near Γ point on the line of Γ - X . The crossed two bands are mainly dominated by $M - d_{z^2}$ and $M - d_{x^2-y^2}$ orbitals, respectively.

Besides, it is found that the location of the 2D Dirac cone k_D is strongly related to the distortion strength. As given in Table I, the Dirac cone shifts far away from Γ point as the increasing of lattice distortion. With the inclusion of SOC, as presented by the local band structures in Fig.2(b) and (e), a general gap is opened with the breaking of the band crossing, which is just a typical image for TIs. Since the distortion does not change the bulk band order, electronic structures are topologically equivalent in so-lattice and distorted-so-lattice. For further confirmation, we also calculated the Z_2 invariant. Though the distortion changes the lattice structure and atomic positions, inversion symmetry is preserved. So parity product at TRIMs is still effective for identifying the topological order [16]. Our calculations found that the Z_2 invariant is 1 for any compound of MX_2 , as shown in Table I. Therefore, distorted-so- MX_2 is still locating at topological non-trivial state.

The SOC effect becoming stronger along with the increasing of atomic weight, and correspondingly, the SOC opened band gap should be also increased. As given in Table I, it is really the case in so-lattice. However, for the distorted-so-lattice, the lattice distortion is also becoming stronger as the increasing of atomic radius. Meanwhile, the band crossing point k_D shifts far away from Γ point, as shown in Table I. Hence, the bulk band gap in the situation with distorted-so-lattice is decided by a competition between the strengths of SOC and lattice distortion. As presented in Table I, the competed result in this series of compounds gives the largest band gap of about 64 meV, appearance in WS_2 .

Because of the non-trivial 2D bulk band order in MX_2 , topological protected metallic edge state happens. For calculation of the edge state, we have constructed the slab model through MLWFs based tight binding method [17–19]. In so-lattice, since the bands around Fermi level are almost consisted by the hybridized $M - d_{z^2}$ and $M - d_{x^2+y^2}$ orbitals for all the compounds of MX_2 , MLWFs are derived from atomic d_{z^2} and $d_{x^2-y^2}$ -like orbitals. While for distorted-so-lattice, due to the difference between lattice constants of a and b , it is not accurate enough to describe the tight binding model by only including d_{z^2} and $d_{x^2-y^2}$ -like orbitals, in which d_{xy} -like orbital is also necessary. The tight binding parameters are determined from the MLWFs overlap matrix. The slab model was constructed in x direction for so-lattice due to the cubic symmetry, and both of x and y directions were choose for distorted-so lattice, corresponding projected 1D-BZ given in Fig.1 (e). In order to eliminate the coupling between two edges, the widths of the slabs were up to 200 and 100 unit cells for MoS_2 and WS_2 , respectively.

From Fig.3 we can see that edge states exist for both so-lattice and distorted-so-lattice. While the details are depending on different compounds and edge terminations. For example, edge bands cut Fermi level three

times for so- WS_2 , whereas other cases just cut Fermi level once. As the differences of chemical potentials, some cases do not show Dirac point like edge states, but the non-trivial Z_2 invariant guarantees the edge bands always cutting Fermi level odd times.

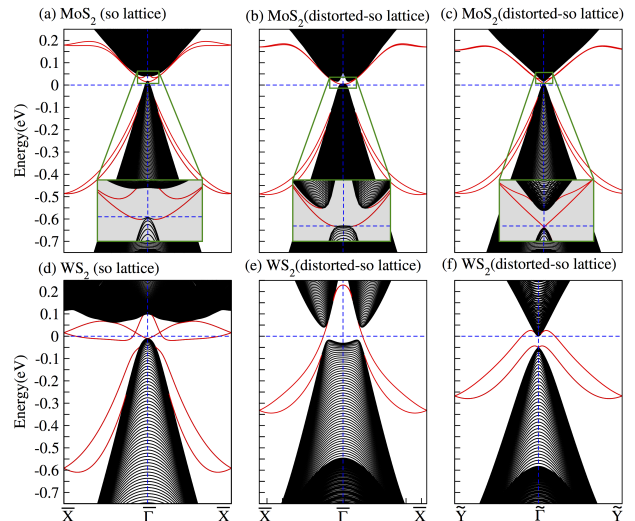


FIG. 3. (color online) Tight binding edge band structures for (a) so- MoS_2 , (b) distorted-so- MoS_2 , (c) so- WS_2 , as well as (d) distorted-so- MoS_2 . Local band structures for MoS_2 around Fermi energy are showing inset. Red curves corresponding to edge states. Fermi energy is set to zero.

As we have discussed above, the effect of SOC is just opening the band gap but not inducing band inversion. Therefore, the physics of band inversion can be understood without SOC. As in the situation of graphene, the band inversion in MX_2 is due to the symmetry protected Van Hove singularity (VHS). In two dimensions, energy band with opposite energy dispersions along different directions can induce the saddle point at the transition momenta, which known as VHS. Moreover, if two bands with VHS cross each other, a band inversion will be there naturally. This is just case in the MX_2 .

From the DFT band structures we have known that, without inclusion of SOC the so-lattice- MX_2 presents as semi-metallic state with degenerated $M - d_{z^2}$ locating at Γ point. This degeneration can be regarded as an overlap of two saddle points belonging the two bands with VHSs, as the schematic showing in Fig. 1(d). After lattice distortion, the character of VHS becomes more obviously due to the symmetry breaking. As presented in Fig. 1(e), the two neighboring bands shifts upwardly and downwardly, respectively, and overlapped two saddle points are separated by a band gap around Γ point. The features of VHS are also obviously in the local DFT band structures as given in Figs. 2 (a, b) and (d, e). Besides, according to the density of states (DOS) expression in lattice momentum space, $g(E) \propto \int \frac{dk_i}{(\nabla_{k_j} E)}$ (where, $g(E)$

is the DOS at energy E , and $i, j=x, y$), DOS integrand at the saddle point diverges due to the extreme of energy dispersion. The diverged peaks can be found in the DOS for both MoS₂ and WS₂, as presented in Fig2.(c) and (f).

Furthermore, as we have seen in the DFT band structures, the lattice distortion also shifts the degenerated point away from Γ point. Similar to graphene, the new degenerated point exhibits as a massless Dirac cone, and the only difference is the location difference of the Dirac cone in lattice momentum space. In graphene, the Dirac cones paired locate at the high symmetry momentas of K and K' , which are connected by inversion and time reversal symmetry. While in distorted-so- MX_2 , Dirac cones paired locate at k_D on the line of $X-\Gamma-X$, which are also connected by inversion and time reversal symmetry, as shown in Fig. 4(b) and (c). SOC is strong enough to open a considerable bang gap in distorted-so- MX_2 , different from the case of graphene with very weak SOC [21].

In conclusion, by first principles calculations we have theoretically proposed a series of QSH insulators in the allotropes of monolayer TMD MX_2 (with $M=Mo, W; X=S, Se$ and Te). The ground states in the allotropes show distorted-so-lattice. Similar to graphene, the band inversion is induced by symmetry protected VHS, and SOC just plays the role of opening band gap. However, due to much stronger SOC effect in MX_2 , the inverted band gaps are big enough for measurement. The band gap is about 12 meV in MoS₂. And the largest band gap in this series QSH insulators is about 64 meV, which appears in WS₂. The QSH phase in MX_2 broaden the physical properties for DMTCs. As the so and distorted-so phase are derived from the grain boundary of h-MoS₂ monolayers, it is possible to experimentally detect the QSH phase in MoS₂ and the other TMD materials through measuring the current or photo emission on their boundary. In addition, the VHS points indicate the existence of Lifshitz transition in the Fermi surface [22] and might promise interesting superconductivity in these materials.

We are grateful to Z. Wang, C.-X. Liu, H. Su for fruitful discussion.

* Corresponding author:yan@cpfs.mpg.de

- [1] K. S. Novoselov, A. K. Geim, S. V. Morozov, D. Jiang, Y. Zhang, S. V. Dubonos, I. V. Grigorieva, A. A. Firsov, *Science*, **306**, 666, (2004).
- [2] A. H. Castro Neto, F. Guinea, N. M. R. Peres, K. S. Novoselov and A. K. Geim, *Rev. Mod. Phys.* **81**, 109, (2009).
- [3] A. Splendiani, L. Sun, Y. Zhang, T. Li, J. Kim, C.-Y. Chim, G. Galli, and F. Wang, *Nano Letters* **10**, 1271 (2010)
- [4] K. Mak, C. Lee, J. Hone, J. Shan, and T. Heinz, *Phys. Rev. Lett.* **105**, 136805, (2010).
- [5] D. Xiao, G.-B. Liu, W. Feng, X. Xu, and W. Yao, *Phys. Rev. Lett.* **108**, 196802 (2012).
- [6] M. Z. Hasan and C. L. Kane, *Rev. Mod. Phys.* **82**, 3045, (2010).
- [7] Xiao-Liang Qi and Shou-Cheng Zhang, *Rev. Mod. Phys.* **83**, 1,57, (2011).
- [8] S. Najmaei, Z. Liu, W. Zhou, X. Zou, G. Shi, S. Lei, B. I. Yakobson, J.-C. Idrobo, P. M. Ajayan, and J. Lou, *Nat. Mater.* **12**, 754 (2013).
- [9] A. M. van der Zande, P. Y. Huang, D. A. Chenet, T. C. Berkelbach, Y. You, G.-H. Lee, T. F. Heinz, D. R. Reichman, D. A. Muller, and J. C. Hone, *Nat. Mater.* **12**, 554 (2013).
- [10] Z. Zhang, X. Zou, V. H. Crespi, and B. I. Yakobson, *ACS Nano* **7**, 10475 (2013).
- [11] Weifeng Li, Meng Guo, Gang Zhang, and Yong-Wei Zhang, *Phys. Rev. B.* **89**, 205402 (2014).
- [12] H Terrones and M Terrones, *2D Mater.* **1**, 011003 (2014).
- [13] G. Kresse and J. Hafner, *Phys. Rev. B* **48**, 13115, (1993).
- [14] G. Kresse and J. Furthmüller, *Comp. Mater. Sci.* **6**, 15 (1996).
- [15] J. P. Perdew, K. Burke, and M. Ernzerho, *Phys. Rev. Lett.* **77**, 3865 (1996).
- [16] Liang Fu and C. L. Kane, *Phy. Rev. B.* **76**, 045302 (2007).
- [17] N. Marzari and D. Vanderbilt, *Phys. Rev. B* **56**, 12847 (1997).
- [18] I. Souza, N. Marzari, and D. Vanderbilt, *Phys. Rev. B* **65**, 035109 (2001).
- [19] A. A. Mostofi, J. R. Yates, Y. S. Lee, I. Souza, D. Vanderbilt, and N. Marzari, *Comput. Phys. Commun.* **178**, 685 (2008).
- [20] C. Franchini, R. Kovik, M. Marsman, S. S. Murthy, J. He, C. Ederer, and G. Kresse, *J. Phys.: Condens. Matter* **24**, 235602 (2012).
- [21] C. L. Kane and E. J. Mele, *Phy. Rev. Lett.* **95**, 226801, (2005).
- [22] I. M. Lifshitz, *Sov. Phys. JETP* **11**, 1130 (1960).